Mon. Not. R. Astron. Soc. **398,** 575–582 (2009) doi:10.1111/j.1365-2966.2009.15139.x

Does heating by AGN shocks affect abundance profiles in galaxy clusters?

F. Xiang,[1⋆] E. Rudometkin,[2] E. Churazov,[1,2] W. Forman[3] and H. Böhringer[4]

[1]*Max-Planck Institut für Astrophysik, Karl-Schwarzschild-Strasse 1, 85741 Garching, Germany*
[2]*Space Research Institute (IKI), Profsoyuznaya 84/32, Moscow 117997, Russia*
[3]*Harvard–Smithsonian Center for Astrophysics, 60 Garden St., Cambridge, MA 02138, USA*
[4]*MPI für Extraterrestrische Physik, PO Box 1603, 85740 Garching, Germany*

Accepted 2009 May 22. Received 2009 May 13; in original form 2008 September 8

ABSTRACT

We evaluate the impact of gas shock heating by a central active galactic nuclei (AGN) in M87 on the radial distribution of heavy elements. The propagation of a shock creates an inverted entropy profile, and the subsequent rearrangement of the gaseous atmosphere transports metal-rich gas from the central region to larger radii. We show that for the parameters of the relatively weak shock, recently found in M87, the abundance profile is not strongly affected by the redistribution of the shock heated gas (except for the very central region). At the same time, the energetics of the source is fully sufficient to broaden the metal distribution to match the observations, strongly suggesting that mechanisms other than direct shock heating must operate in cluster cores. The absence of a very strong abundance peak at the very centre of M87 suggests that the central AGN produces frequent (every few 10 Myr) and relatively weak outbursts, rather than rarer (every few 100 Myr) and an order of magnitude more powerful events.

Key words: galaxies: abundances – galaxies: clusters: general.

1 INTRODUCTION

X-ray spectroscopy is routinely used to determine the metallicity of the hot gas in galaxy clusters and groups. The gas metallicity contains the record of metals produced by stars and injected into the hot medium by supernova (SN) explosions and stellar winds. The gas metallicity is a particularly important diagnostic for cool core clusters whose heavy metal abundances are strongly peaked at the centre (e.g. Böhringer et al. 2004; De Grandi et al. 2004). These clusters always have a very bright galaxy (BCG) dwelling in their centres, which makes the stars in BCGs a prime candidate for producing the peaked abundance profiles that are observed.[1] The total amount of metals, in particular iron, in cool cluster cores seems to be consistent with this assumption (e.g. Böhringer et al. 2004). The observed distribution of iron is, however, broader than the light distribution of the central galaxy. This suggests that the gas does not form a perfectly static atmosphere, but is instead involved in motions, that transport metals to larger radii. All cool core clusters contain a supermassive black hole [an active galactic nuclei (AGN)] in the BCG at the cluster centre which is believed to be the source of energy for the cooling gas (e.g. McNamara & Nulsen 2007, and references therein). AGN activity is also a natural candidate for generation of the gas motions and the metal distribution has been used to constrain the AGN/gas interactions (e.g. Rebusco et al. 2005, 2006; Heath, Krause & Alexander 2007; Roediger et al. 2007; David & Nulsen 2008).

Here, we consider the impact of AGN-generated shock heating on the metal distribution in cool core clusters. A shock, driven by an AGN outburst, creates an inverted entropy profile in cluster gaseous atmospheres. The subsequent gas redistribution causes highly enriched gas from the core to move towards larger radii. Motivated by the accurate determination of the shock parameters in M87 using long *Chandra* observations (Forman et al. 2005, 2007, 2009), we focus on M87 and evaluate the efficiency of this redistribution process.

⋆E-mail: feiart66@gmail.com

[1]Ram-pressure stripping is another mechanism, which is often discussed in relation to centrally concentrated abundance profiles (see Schindler & Diaferio 2008, and references therein). We do not consider ram-pressure stripping here. This is at least partly justified since we concentrate on the particular case of a very large elliptical galaxy M87, which strongly dominates its environment up to a distance of ∼100 kpc.

2 INITIAL CONDITIONS: M87 DENSITY AND TEMPERATURE PROFILES

For initial conditions, we used the electron density n_e and temperature T_e profiles derived from long *Chandra* observations of M87 (Churazov et al. 2008; Forman et al. 2009). Namely

$$n_e = 0.22 \times \left[1 + \left(\frac{r}{r_c}\right)^2\right]^{-\frac{3}{2}\beta} \quad \mathrm{cm}^{-3}, \tag{1}$$

where $\beta = 0.33$ and $r_c = 0.93$ kpc, and

$$T_e = 1.55 \times \left[1 + \left(\frac{r}{10.23\ \mathrm{kpc}}\right)^2\right]^{0.18}\ \mathrm{keV}. \quad (2)$$

These expressions describe reasonably well the best-fitting parameters of the deprojected *Chandra* spectra over the range of radii from ∼1 up to ∼40 kpc, and broadly agree with the *XMM–Newton* data (Matsushita et al. 2002). Note, however, that deprojected *Chandra* spectra were approximated by a single temperature Astrophysical Plasma Emission Code (APEC) model and the best-fitting parameters may be subject to various biases in the central region where multitemperature gas is present. Another caveat is that the gas in M87 is already disturbed by the shock and bubbles of relativistic plasma (e.g. Forman et al. 2005, 2007), but we nevertheless use the fits to the observed profiles as the 'pre-outburst' initial conditions for subsequent simulations of the shock propagation. In future work, we will address this issue with a full three-dimensional simulation of the outburst in the M87 atmosphere.

3 PRODUCTION OF METALS

Metals in elliptical galaxies, dominated by old stellar populations at the present epoch, are produced by Type Ia supernova (SNIa) explosions and winds of evolved stars. We assume that the metal production rate follows the optical light distribution of the galaxy. Any possible dependencies of SN rates or stellar wind metallicities as a function of radius are ignored. For the metal production rate, we use a similar prescription to that of Böhringer et al. (2004) and Rebusco et al. (2006, also see references therein). For the SNIa rate, we used the latest data of Mannucci et al. (2008) for early type galaxies in clusters: $6.6 \times 10^{-14}\,\mathrm{yr}^{-1}\,\mathrm{M}_\odot^{-1}$ (normalized per unit solar mass of the stellar population) and assume that each SN yields $0.7\,\mathrm{M}_\odot$ of iron to the ICM. For the stellar mass-loss rate, we use the normalization of Ciotti et al. (1991) for the 10 Gyr old stellar population: $\dot{\zeta} = 2.5 \times 10^{-11}\,\mathrm{M}_\odot\mathrm{yr}^{-1}\mathrm{L}_{\odot,B}^{-1}$ (per unit B-band stellar luminosity). We assume that iron comprises a fraction 2.8×10^{-3} of the stellar mass loss. For simplicity, we assume that both SNIa and stellar mass-loss scale with time as $(\frac{t}{10\ \mathrm{Gyr}})^{-1}$, where t is the age of the stellar population (by assumption with a present age of $t = 10$ Gyr). While these time dependencies can be different (see e.g. Renzini et al. 1993), it is not very important for our calculations since the time-scales we consider are short compared to the evolutionary time-scales. In all our calculations, t varies between 5 and 10 Gyr. With these prescriptions and for a stellar mass of M87 of $M_* = 2.0 \times 10^{11}\,\mathrm{M}_\odot$ and a B-band luminosity of $L_B = 6.4 \times 10^{10}\,\mathrm{L}_\odot$, the total iron enrichment rate is

$$\dot{\zeta}_{\mathrm{Fe}} = 1.4 \times 10^{-2}\left(\frac{t}{10\ \mathrm{Gyr}}\right)^{-1}, \quad \mathrm{M}_\odot\ \mathrm{yr}^{-1}, \quad (3)$$

which accounts for SNIa explosions and stellar winds. The stellar wind mass-loss rate is

$$\dot{\zeta} = 1.6\left(\frac{t}{10\ \mathrm{Gyr}}\right)^{-1}, \quad \mathrm{M}_\odot\ \mathrm{yr}^{-1}. \quad (4)$$

With these definitions, the iron abundance in the gas supplied by stars is

$$z_{\mathrm{Fe}} \approx \frac{\dot{\zeta}_{\mathrm{Fe}}}{\dot{\zeta}}\frac{1}{A_{\mathrm{Fe}} \times z_{Fe,\odot}} = 5.3, \quad (5)$$

relative to the solar photospheric abundance. In the above expression, $A_{\mathrm{Fe}} = 56$ is the atomic weight of iron and $z_{\mathrm{Fe},\odot} = 2.95 \times 10^{-5}$ is the solar abundance of iron according to Lodders (2003) (see also Asplund et al. 2000). This value sets the maximum abundance which can be reached under the above assumptions.[2] As long as the abundance is lower than this value, the supply of hydrogen by stellar winds can be neglected in the estimates (as we describe below). The high value of the iron abundance predicted by equation (5) contrasts with X-ray observations of elliptical galaxies – the problem known in the literature as the 'iron discrepancy' (e.g. Renzini et al. 1993; Arimoto et al. 1997). While lowering the SNIa rate and/or the iron mass per explosion can partly remedy the discrepancy, this decrease may, in turn, exacerbate the problem of producing enough iron by cD galaxies in the cores of rich clusters (see iron mass estimates in Böhringer et al. 2004).

Apart from the iron produced by SNIa and stellar winds during late evolution of an elliptical galaxy, the gas can be already enriched by SNII explosions during the early phases of the galaxy/cluster formation. The contribution of this component to the observed central abundance is estimated to be at the level of 10–20 per cent (e.g. Finoguenov et al. 2002; Böhringer et al. 2004). Therefore, we ignore the contribution of this component here (see also footnote in Section 7.3).

The initial radial distribution of iron $\dot{\zeta}(r)$, produced by stars and SNe, should follow the light distribution of the galaxy, modelled as a Hernquist profile (Hernquist 1990). Thus, the iron production rate per unit volume is

$$\dot{\zeta}_{\mathrm{Fe}}(r) = \frac{\dot{\zeta_{\mathrm{Fe}}} M_*}{2\pi}\frac{a}{r}\frac{1}{(r+a)^3}, \quad (6)$$

where $a = \frac{R_{\mathrm{eff}}}{1.8153}$. For M87, we set $R_{\mathrm{eff}} = 7.8$ kpc. The observed light distribution in M87 (e.g. Romanowsky & Kochaneck 2001) is slightly more peaked than the Hernquist profile with these parameters in the inner ∼30 arcsec. Since we are mostly interested in the gas and metal distributions at larger radii, this minor difference does not affect our results.

The M87 light distribution is much more concentrated than the gas density distribution. Therefore, the production of metals in a static atmosphere will lead to a peaked abundance profile. As shown in Fig. 1, the expected cumulative abundance profile after a time interval Δt in a static atmosphere is more sharply peaked than the observations. The cumulative abundance was evaluated as the ratio of the amount of iron produced within a sphere of radius R during a time Δt to the total amount of hydrogen within the same sphere. This ratio is normalized by the solar abundance of iron, i.e.

$$z_{\mathrm{Fe}}(R) \approx \frac{\int_0^R \dot{\zeta}_{\mathrm{Fe}}(r)\,4\pi r^2\,\mathrm{d}r}{\int_0^R n_{\mathrm{e}}(r)\,4\pi r^2\,\mathrm{d}r}\frac{\frac{n_{\mathrm{H}}}{n_{\mathrm{e}}}}{A_{\mathrm{Fe}} \times z_{Fe,\odot}} \times 10\ \mathrm{Gyr} \times \log\frac{t+\Delta t}{t}, \quad (7)$$

where the hydrogen to electron density ratio is given by $\frac{n_{\mathrm{H}}}{n_{\mathrm{e}}} = 0.827$. Here, we took into account that our assumed time evolution of the metal production rate is $\propto t^{-1}$. This estimate ignores the fact that the maximum abundance which can be provided by the enrichment process, with the above parameters, is limited to a maximum value of 5.3 (equation 5 above).

[2] We note that for another popular choice of solar iron abundance $z_{\mathrm{Fe},\odot} = 4.68 \times 10^{-5}$ (Anders & Grevesse 1989), the abundance, predicted by equation (5), drops from 5.3 to 3.3. This value can be further decreased by another ∼30 per cent if one assumes that an SNIa explosion on average produces $0.5\,\mathrm{M}_\odot$ of iron instead of 0.7.

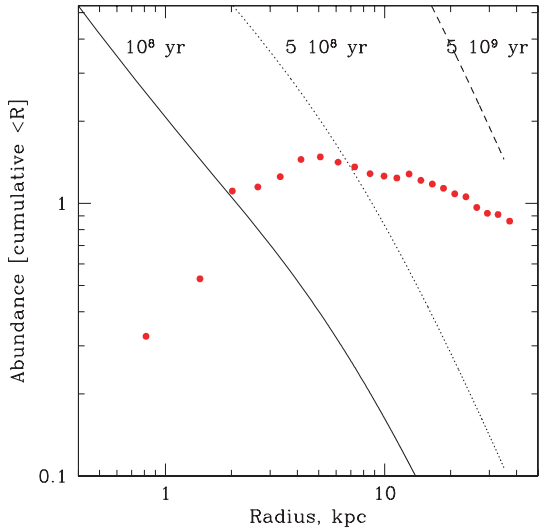

Figure 1. The expected abundance profile, if metals are deposited into a static atmosphere for $10^8, 5 \times 10^8$ and 5×10^9 yr. The maximum abundance which can be produced in our model is 5.3 (corresponding to the top of the plot). For comparison, the cumulative abundance derived from the 1T APEC fits to the deprojected *Chandra* data is shown with red circles. Note that a bias due to the presence of multitemperature plasma (e.g. Buote 2000) may be very significant in the central 5 kpc (1 arcmin) region and 1T best-fitting values may not reflect the true abundance profile here (e.g. Matsushita et al. 2002).

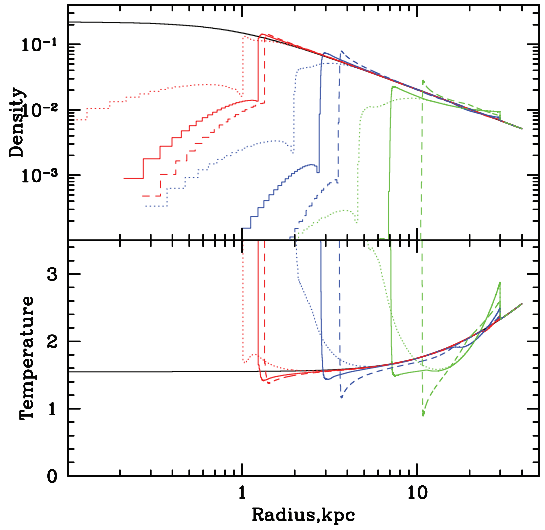

Figure 2. Density and temperature profiles modified by the outburst of a central AGN. Red, blue and green lines correspond to the outburst energy $E_0 = 5 \times 10^{56}, 5 \times 10^{57}, 5 \times 10^{58}$ ergs, respectively. Dotted, solid and dashed lines correspond to outburst duration $\Delta t = 2 \times 10^5, 2 \times 10^6\, 2 \times 10^7$ yr, respectively. Snapshots shown correspond to the time when the leading front of the shock reaches a distance of 30 kpc distance from the centre. The black lines show the initial gas density and temperature profiles.

4 SHOCK MODEL

To model the gas heating by an AGN-driven shock, we used the Lagrangian one-dimensional code (as in Forman et al. 2009). The initial density and temperature profiles were set according to equations (1) and (2). A static gravitational potential $\varphi(r)$ was calculated by requiring the initial density and temperature profiles to satisfy the hydrostatic equilibrium equation. The gas adiabatic index was set to 5/3.

Following Forman et al. (2009), we characterize the AGN outburst with two parameters: total energy E_0 and duration Δt. The AGN power as a function of time is described by a double θ function:

$$L_{\rm AGN}(t) = \begin{cases} 0 & t < 0 \\ \frac{E_0}{\Delta t} & 0 < t < \Delta t. \\ 0 & t > \Delta t \end{cases} \quad (8)$$

We model the radial distribution of energy deposition (per unit volume) as a power-law function of radius:

$$h(r,t) = L_{\rm AGN}(t) \frac{r^{-\alpha}}{\int_0^{R_{\rm AGN}(t)} r^{-\alpha}\, 4\pi r^2\, {\rm d}r}. \quad (9)$$

Thus, the energy is deposited in a few central cells $r < R_{\rm AGN}(t)$: the internal energy in the cells is increased at each time step according to the above equation (9). Initially the outer radius of the region used for energy deposition is $R_{\rm AGN}(0) = 0.5$ kpc. As the radii of the cells grow, the injection region grows accordingly. This was done to mimic the situation when the AGN is inflating a bubble of relativistic plasma at the centre with internal sound crossing time much smaller than the characteristic time of the bubble expansion. The value of α was (arbitrarily) set to 0.5 in the simulations. The properties of the final density and temperature profiles only weakly depend on the particular value of α (as was verified by varying α from 0 to 1).

Guided by the fiducial values derived for the M87 shock from *Chandra* observations (Forman et al. 2007, 2009): $E_0 \sim 5 \times 10^{57}$ ergs and $\Delta t \sim 2 \times 10^6$ yr, we ran a grid of models with bracketing values of E_0 and Δt. Namely, $E_0 = \{5 \times 10^{56}, 5 \times 10^{57}, 5 \times 10^{58}\}$ ergs, duration $\Delta t = \{2 \times 10^5, 2 \times 10^6, 2 \times 10^7\}$ yr– all together nine runs. In the simulations, we follow the shock propagation until the leading front reaches a distance of 30 kpc from the centre. By this time, the shock has become relatively weak and no longer generates much entropy. The choice of this particular radius (30 kpc) is rather arbitrary but our results are insensitive to the actual value.

The gas density and temperature profiles modified by the shock in each of the nine runs are shown in Fig. 2 with coloured lines. For comparison, the initial profiles are shown with the black lines. One can easily identify three distinct regions in the profiles modified by the shock.

Region I. The innermost part of the atmosphere, which corresponds to the region where the energy was directly deposited during the simulations [i.e. gas inside $R_{\rm AGN}(t)$]. As the gas is directly heated in this region (by design of our simulations), it has very high entropy and, as a consequence, has a high temperature and low density. For M87 (and other cooling flows), a more relevant model could be one in which relativistic plasma is injected by an AGN into the central region, rather than direct heating of the gas. For the purpose of this paper this is not a critical issue, since the initial value of $R_{\rm AGN} = 0.5$ kpc is small enough (much smaller than the galaxy effective radius) that only a small fraction of the gas and metals generated by the galaxy lie in this region. For instance, for a pure Hernquist profile with effective radius of 7.8 kpc, only ~1 per cent of the galaxy light is contained within the central 0.5 kpc. In M87, this fraction can be larger (due to a more peaked light profile near the centre), but it is still small.

Region II. Intermediate regions between Region I and the shock front. This is the most important region for the purpose of this

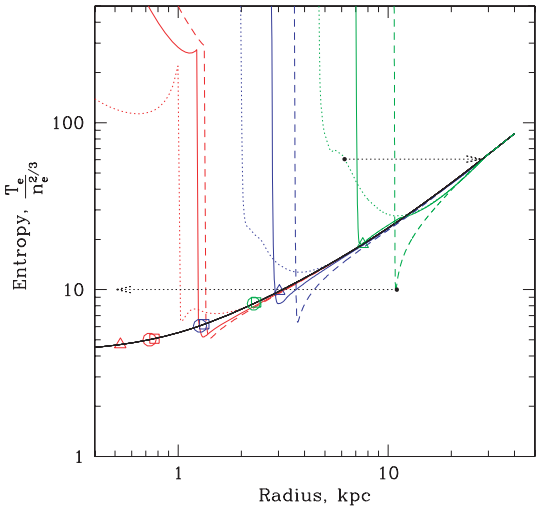

Figure 3. Inversion of the entropy profile caused by shock heating of the central region. The colours and line types are coded similar to Fig. 2. Two black arrows show schematically that heated gas will move towards large radii, while the lowest entropy gas will sink to the centre. For each model, the open triangle, circle and square (for $\Delta t = 2 \times 10^5, 2 \times 10^6\, 2 \times 10^7$yr, respectively) mark the initial radius of the cell which has the lowest entropy at the end of the simulation.

paper. The gas in this region is heated by the shock propagation. If the shock is strong (due to a powerful and short-duration outburst), then the gas is strongly heated. In the opposite case of a weak shock (less powerful and of long duration), the gas in region II is merely displaced by the expanding central Region I, except for a narrow shell immediately adjacent to Region I.

Finally, *Region III* is the region outside the leading shock front (i.e. $r > 30$ kpc in Fig. 2), occupied by undisturbed gas.

The radii separating Regions I and II are visible in Fig. 2 as almost vertical lines, corresponding to a sharp drop of temperature from values above 3 keV to values below 2 keV. The boundary between Regions II and III is by definition at 30 kpc, where the jump in temperature/density is seen.

5 ENTROPY AND ABUNDANCE PROFILES

The gas entropy profiles (to be precise the profiles of the quantity $s(r) = \frac{T_e}{n_e^{2/3}}$) corresponding to the same set of shock models are shown in Fig. 3. When the energy is released into an initially small volume – a relatively strong shock is driven into the cluster gas and it substantially increases the gas entropy. As the shock propagates through the gas and weakens (the density profile is less steep than r^{-2}), the shock becomes less efficient at entropy generation. As a result an inverted entropy profile is created, as seen in Fig. 3. For 'short'-duration outbursts the entropy increase is more pronounced since such outbursts generate stronger shocks. The corresponding profiles have extended minima. For 'long'-duration outbursts, the gas is merely displaced by expanding Region I (as explained above) and the corresponding profiles are characterized by narrower and deeper minima.

6 REARRANGEMENT OF THE ATMOSPHERE AND RESULTING ABUNDANCE PROFILES

An atmosphere with an inverted entropy profile (as shown in Fig. 3) is unstable and must pass through a rearrangement phase which will restore the atmosphere to one with a non-decreasing (with radius) entropy profile. Low-entropy gas will tend to sink to the centre of the cluster, while high-entropy gas will instead move towards larger radii as shown by the dotted arrows in Fig. 3. After a few dynamical times (few 10^7 yr), the atmosphere will come to a stable equilibrium. Since the dynamical time is short compared to the cooling or enrichment time-scales, we assume that for the purposes of studying the evolution of the heavy elements, the rearrangement is instantaneous. The rearrangement process is very complex since gas lumps with different entropies can mix during the gas motion. We will completely ignore these complications and assume that the gas mass distribution over entropy remains unchanged during rearrangement. We also neglect (for the purpose of our simple model) the potential energy released during rearrangement process.[3] Namely, we model rearrangement as follows. From our shock simulations, we have the gas mass m_i, iron mass $m_{\mathrm{Fe},i}$ and the entropy s_i for each of the $i = 1, n$ simulated cells. We then rearrange the cells (and associated masses) to produce a stable atmosphere, i.e. entropy increasing with radius (cell index). We now solve the hydrostatic equilibrium equation

$$\frac{1}{\rho}\frac{\mathrm{d}P}{\mathrm{d}r} = -\frac{\mathrm{d}\varphi}{\mathrm{d}r}, \tag{10}$$

with the boundary condition that the pressure at the outer boundary is equal to $P(r_n) = P_{\mathrm{out}}$. A similar approach was used by Kaiser & Binney (2003). We start with an initial estimate of the pressure at the centre of the cluster P_{c} and calculate the density of the first cell as $\rho_1 \propto (\frac{P_{\mathrm{c}}}{s_1})^{3/5}$. We then integrate equation (10) over one cell to get the pressure for the next cell and repeat the procedure for the next cell. The pressure in the outmost shell $P(r_n)$ is compared with P_{out}. If they do not match, then P_{c} is adjusted and the whole procedure repeats until agreement is reached (the order of cells remains unchanged during this procedure). If the outer boundary is sufficiently far from the region affected by the shock, then the behaviour of the solution in the inner region does not depend much on the radius r_n used for the outer boundary condition $P(r_n) = P_{\mathrm{out}}$. The outcome of this procedure is a new stable configuration for the atmosphere with a known gas mass and iron mass for each shell composing this atmosphere.

Since the shock preferentially heats the inner regions, where most of metals are produced, the exchange of gas parcels with high and low entropies causes high-metallicity gas in the very core to be replaced with less metal rich gas from larger radii. The resulting (cumulative) abundance profiles for each of the shock models are shown in Fig. 4.

7 DISCUSSION

7.1 Effect of shock strength and outburst energy on the M87 abundance profile

As is clear from Fig. 4, for all models the abundance profiles develop a characteristic core at the centre. The dilution of the small mass of highly enriched core gas by a larger mass of comparable entropy gas from larger radius contributes to the formation of a central flat core. The radial extent of the core (and the maximal abundance) is a function of the minimum entropy present in the system after the

[3]While heating certainly occurs during the rearrangement process, we intentionally limit our consideration to the entropy generation at the shock front only.

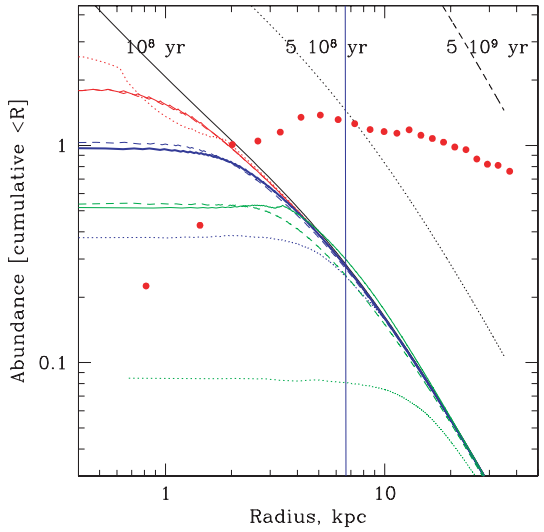

Figure 4. Modification of the cumulative abundance profiles after the atmosphere restores a stable configuration (entropy increasing outwards, as described in the text). The total mass of iron is conserved and it is, therefore, the same for all colour curves. The decrease of abundance in the central region is compensated by a slight increase of the abundance at larger distances from the centre. The thick solid blue curve corresponds to the best-fitting shock parameters ($E_0 \sim 5 \times 10^{57}$ ergs and $\Delta t \sim 2 \times 10^6$ yr) for M87 (Forman et al. 2007). The blue vertical line shows the $R = 6.6$ kpc radius of the sphere within which the gas can be mixed if the energy $E_0 \sim 5 \times 10^{57}$ ergs is used to raise the entropy of the gas inside the sphere to the value characteristic for the gas just outside this sphere. The cumulative abundance profile derived from *Chandra* data is shown with red points.

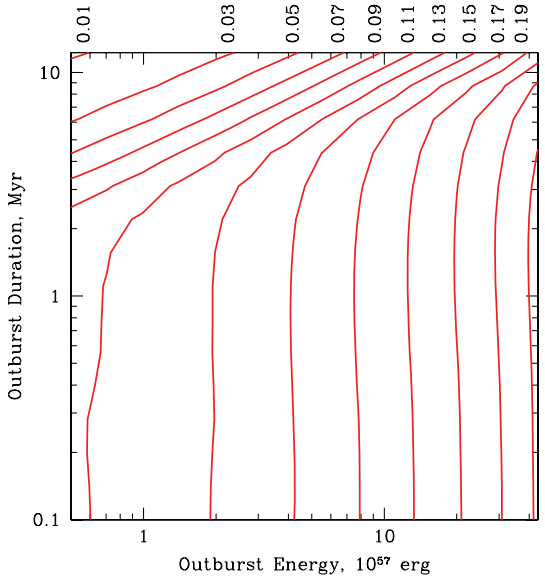

Figure 5. The fraction of the outburst energy (contours) escaping from the central 30 kpc region with the expanding shock as a function of the outburst total energy (x-axis) and the outburst duration (y-axis). The actual fraction associated with each contour is shown by a label at the top of the plot. The energy escaping from 30 kpc region was evaluated by calculating the kinetic energy of the gas at the time when the shock front was at 30 kpc from the centre and multiplying this value by 2. This is a crude estimate which assumes that we deal with a simple weak plane wave having total energy twice its kinetic energy.

passage of the shock, which is in turn a function of the outburst energy E_0 and outburst duration Δt. The more powerful and short the outburst, the larger is the core of the abundance profile. From *Chandra* observations of M87, Forman et al. (2007, 2009) argued that the recent (∼10 Myr old) major outburst was best described by $E_0 \sim 5 \times 10^{57}$ ergs and $\Delta t \sim 2 \times 10^6$ yr. The key observables are the radius of the shock $R \sim 13$ kpc and the jump in temperature/density at the shock front. The amplitude of the jump suggests the present Mach number of the shock ∼1.2 (see Forman et al. 2007 for details). These figures already provide a reasonable estimate of the total energy in the outburst, which drove the observed shock. The duration of the outburst was estimated through the comparison of the shock and the central cavity region (Forman et al. 2009). These parameters correspond to the blue solid line in Fig. 4. One can see that the radius of the abundance core is only ∼1–2 kpc i.e. after a single outburst the metals stay well within the effective radius of the galaxy where they are produced.[4] This rather small impact on the abundance distribution is a direct consequence of a rather 'mild' outburst, which does not significantly change the gas entropy (except for a very small region in the centre).

The gas cooling time at the centre of M87 is $t_{\rm cool,0} \sim 10^8$ yr. It was evaluated as $t_{\rm cool} = \frac{5/2(n_{\rm e}+n_i)kT}{n_{\rm e}n_i\,\Lambda(T)}$ using the cooling function $\Lambda(T)$ from Sutherland & Dopita (1993) with $T_{\rm e} = 1.55$ keV, $n_{\rm e} = 0.2\,{\rm cm}^{-3}$ and solar metallicity. Thus, to avoid a cooling catastrophe the characteristic time between outbursts $t_{\rm rep}$ has to be shorter than the cooling time, i.e. $t_{\rm rep} \lesssim t_{\rm cool,0} = 10^8$ yr.

On the other hand, the cooling time at 50 kpc is ∼10^{10} yr and the total radiative losses of the gas inside the same radius are $L_{\rm cool} \sim 1.3 \times 10^{43}\,{\rm erg\,s^{-1}}$. Assuming that this 50 kpc region is a 'cooling flow region' in M87 and radiative losses inside 50 kpc are replenished by AGN outbursts (with an efficiency of converting outburst energy to heat close to 1 as suggested by Fig. 5), we can estimate the energy required from a single outburst:

$$E_1 = L_{\rm cool} \times t_{\rm rep} = 4 \times 10^{58} \left(\frac{t_{\rm rep}}{10^8\ {\rm yr}}\right)\ {\rm ergs}. \qquad (11)$$

Such outbursts would have stronger impact on the abundance profile. The *Chandra* data (Forman et al. 2007, 2009) suggest that an order of magnitude less powerful outburst occurred about 10^7 yr ago. If such outbursts are typical for M87, then a more plausible scenario would be ∼10 times more frequent outbursts, i.e. $t_{\rm rep} \approx 10^7$ yr $\approx 0.1 \times t_{\rm cool,0}$ and ∼10 times less powerful outbursts. The shock heating from these weak outbursts would have little impact on the abundance profiles outside ∼2 kpc.

One can also use the abundance peak (or lack of a peak) at the centre of M87 to constrain the interval between the outbursts $t_{\rm rep}$. Indeed, in 10^8 yr, the metal injection by stars increases the abundance at 1 and 2 kpc distances from the galaxy centre by 2 and 1 solar values, respectively (see Fig. 1 or 4). Thus, the absence of a very sharp abundance peak in the very core of M87, by itself, means that outbursts must occur often. If one could reliably measure the abundance difference at two radii (1 and 2 kpc), then the expected difference in abundances will be $\Delta z \sim (\frac{t_{\rm last}}{10^8\ {\rm yr}})$, where $t_{\rm last}$ is the elapsed time since the latest major outburst. There are two caveats associated with this estimate. First, the central part of M87 is exactly the region where reliable abundance determination is observationally difficult. Second, the same region is currently undergoing an outburst and any estimate cannot be very accurate. Nevertheless, the mere absence of an abundance spike in the very core of M87 is best explained by frequent (and weak) outbursts.

[4]The impact of multiple outbursts is discussed later.

Qualitatively a similar conclusion was reached by Simionescu et al. (2008) based on the analysis of *XMM–Newton* observations of M87. They measured the abundance of iron and other elements in the cool gas which is believed to be enriched by stars near the very core of M87 and then uplifted to larger radii by buoyant bubbles of relativistic plasma. From measured abundances, Simionescu et al. (2008) concluded that the enrichment time of the cool gas (analogous to the $t_{\rm rep}$ above) is somewhere between 30 and 100 Myr.

7.2 Energetically more efficient mixing

The above model assumes that entropy generation (i.e. heating) occurs exclusively at the shock fronts. By design of our simulations, the subsequent rearrangement of the gas layers conserves entropy and the excess potential energy released during the rearrangement process is neglected. It is interesting to consider a more energetically efficient mixing scenario when the available energy E_0 is used to create a flat entropy profile within a sphere with radius $R_{\rm mix}$. The resulting distribution will be neutrally stable and mixing can proceed over the whole volume of the sphere. We can calculate the energy needed to *instantaneously* heat the gas at each radius to produce a flat entropy profile to a radius $R_{\rm mix}$:

$$E_0 = \int_0^{R_{\rm mix}} \frac{nkT}{\gamma - 1} \frac{s(R_{\rm mix}) - s(r)}{s(r)} 4\pi r^2 \, {\rm d}r. \quad (12)$$

Solving the above equation for $R_{\rm mix}$ we find that for $E_0 \sim 5 \times 10^{57}$ ergs, a flat entropy profile can be generated within $R_{\rm mix} = 6.6$ kpc. Except for the factor $\frac{s(R_{\rm mix})-s(r)}{s(r)}$, the expression under the integral is the gas thermal energy. For realistic conditions, the dominant contribution to the integral comes from the radial range $r \sim R_{\rm mix}$. The factor $\frac{s(R_{\rm mix})-s(r)}{s(r)} \sim 1$ and for simple estimates it can be dropped from equation (12). For M87 (over the range of E_0 of interest here, i.e. for $E_0 \sim 5 \times 10^{57}$ ergs), omitting this entropy factor introduces an error of less than a factor of 2 in $R_{\rm mix}$ and changes $R_{\rm mix}$ from 6.6 to 4.6 kpc. The above estimate essentially says that to mix the gas within a radius $R_{\rm mix}$, one needs to deposit an amount of energy comparable to the gas thermal energy within a volume $R_{\rm mix}$.[5]

The resulting radius $R_{\rm mix}$ over which the gas is mixed is much larger than the 1–2 kpc core in the abundance distribution produced by shock heating for our fiducial set of outburst energies and durations. We emphasize that this 'inefficiency' of gas mixing is not due to a large fraction of outburst energy escaping from the cooling flow region with the outgoing shock/sound wave. In fact, for the outburst parameters favoured by the *Chandra* data, only a small fraction, less than 20 per cent (see Fig. 5), is carried away from the central 30 kpc region by the outgoing shock. Instead, for a moderately powerful and long duration outburst ($E_0 \sim 5 \times 10^{57}$ ergs and $\Delta t \sim 2 \times 10^6$ yr), the bulk of the energy goes into the enthalpy of a central, very high entropy volume/cavity. In the mixing scenario described by equation (12), the same amount of energy E_0 is spread over a much larger volume allowing for large masses of gas to be mixed. The very same arguments imply that not only gas mixing, but also gas heating by shocks is inefficient. As discussed by Churazov et al. (2001, 2002; see also Begelman 2001; Nulsen et al. 2007), the energy stored as enthalpy of the central cavity can be used for efficient gas heating during the rise of the buoyant cavity through the cluster atmosphere. The final heating efficiency (entropy generation) in this model is high, but this heating is not directly related to the entropy generation at the front of the original shock. For instance, one can think of the gas turbulent motions excited during the rearrangement process, which eventually decay and heat the gas. Similarly, one can expect that the same mechanism will increase the mixing efficiency. The mixing induced by jets and buoyant bubbles was, in particular, studied in numerical simulations by Roediger et al. (2007) and Heath et al. (2007). They found that jets and bubbles can indeed disperse metals through the inter-cluster medium (ICM). Thus, while shock by itself may not be an efficient channel of heating/mixing the ICM, eventually much of the energy deposited by the AGN can be used to mix/heat the gas.

[5] We stress that in general the above estimate does not correspond to the minimum energy required to mix the gas within a given sphere. This is simply one possible way, not necessarily the most efficient, to promote mixing.

7.3 Toy mixing model

Starting from the assumption that the gas heating efficiency and metal mixing are linked to each other, we can build a simple toy model of metal mixing in cluster cooling cores.

Let us assume that the time averaged AGN mechanical power $L_{\rm AGN}$ matches approximately the gas cooling losses integrated over the cooling flow region. For M87, this means $L_{\rm AGN} \sim$ few $\times 10^{43}$ ergs s^{-1}. We further assume, along the lines of the arguments presented above, that the gas mixing efficiency induced by the AGN follows equation (12). If the AGN was active for a time interval τ, then the gas is uniformly mixed inside a sphere with radius $\Re(\tau)$ such that the gas thermal energy inside the sphere matches the AGN power released during a period τ:

$$\tau \times L_{\rm AGN} = \int_0^{\Re(\tau)} \frac{nkT}{\gamma - 1} 4\pi r^2 \, {\rm d}r. \quad (13)$$

This equation is essentially equation (12), where we have omitted the factor $\frac{s(\Re)-s(r)}{s(r)}$ for the sake of simplicity (given the qualitative level of these estimates).

With the above prescription, a short period of AGN activity will cause gas mixing inside a small sphere while a long period of activity mixes the gas in a larger sphere. In particular, during one cooling time, the gas inside a cooling radius is mixed. Thus, metals produced about one cooling time ago will be dispersed over the whole cooling flow region, while more recently produced metals are mixed within a smaller sphere. Assuming that the AGN was active for a period of time from t_1 to t_2, the total mass of iron within a sphere with radius R can be evaluated as

$$M_{\rm Fe}(< R) = \int_{t_1}^{t2} {\rm d}t \; A(t, R), \quad (14)$$

where

$$A(t, R) = \begin{cases} \frac{M_{\rm gas}(<R)}{M_{\rm gas}(<\Re(t))} \int_0^{\Re(t)} \dot{\zeta}_{\rm Fe}(r) \, 4\pi r^2 \, {\rm d}r & \Re(t) > R \\ 0 & \Re(t) < R. \end{cases} \quad (15)$$

Here, $\Re(t)$ is evaluated using equation (13). The expected abundance profiles for different values of the AGN mechanical power are shown in Fig. 6. For this figure, we set t_1 and t_2 to 0.5 and 10 Gyr, respectively. Clearly within our toy model, the AGN power of 10^{44} ergs s^{-1} would mix metals over very large regions (perhaps beyond the valid range of the density and temperature profiles used

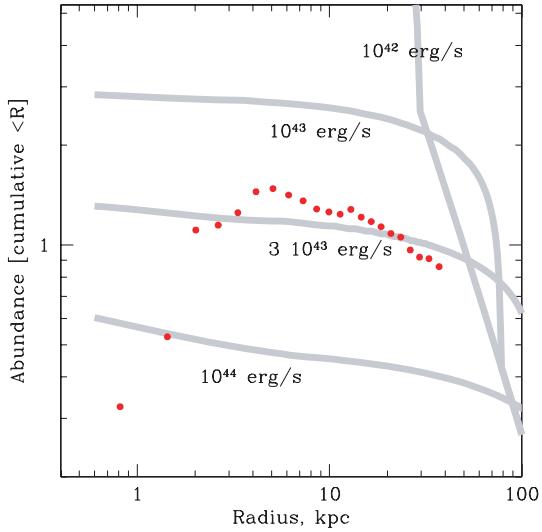

Figure 6. Abundance profile in the toy model for different AGN outburst powers. The grey curves are the predicted abundance distributions according to equation (14) for $L_{\rm AGN} = 10^{42}$, 10^{43}, 3×10^{43} and 10^{44} erg s^{-1} from top to bottom, respectively.

here) resulting in very low metal abundances in the core.[6] An AGN power of 10^{42} ergs s^{-1} would instead produce very little mixing and in the central ∼20–30 kpc the abundance will be ∼5 solar. An AGN power of the order of $L_{\rm AGN} =$ few $\times\ 10^{43}$ ergs s^{-1} yields an abundance level which approximately matches the observations. Therefore, we conclude that in our toy model, a time average energy input of the order of a few $\times\ 10^{43}$ ergs s^{-1} is needed to explain the M87 abundance profile. This energy input, within a factor of 2 (depending on the definition of the cooling radius), coincides with the gas cooling losses in M87. Given the simplicity and obvious crudeness of our estimates, we conclude that the model is reasonably successful in reproducing the basic characteristics of M87.

The comparison of the abundance core of 1–2 kpc expected in a pure shock heating model (for $E_0 \sim 5 \times 10^{57}$ ergs and $\Delta t \sim 2 \times 10^6$ yr) and $R_{\rm mix} = 6.6$ kpc expected from equation (12) ($R_{\rm mix} =$ 4.6 kpc from equation 13) suggests that our toy model is considerably more efficient at metal mixing. An energy of order a few $\times$ 10^{56} ergs would be sufficient to mix the gas inside 1–2 kpc if equation (12) or (13) applies. Extrapolating this difference in efficiency to the multiple explosions, we can conclude that at least an order of magnitude larger time averaged AGN power (few $\times\ 10^{44}$ ergs s^{-1}) would be needed in M87 to provide mixing that is driven purely by shock heating.

Of course, the above toy model cannot even approximately describe the process of metals spreading through the inter-stellar medium (ISM)/ICM. The model is built around a single assumption that a deposition of a given amount of energy into the gas leads to the gas mixing within the sphere containing a similar amount of thermal energy. All other complications including gas cooling, physics of gas heating, process of mixing are neglected. Nevertheless, we believe that our toy model can serve as an order of magnitude approximation of a mixing process mediated by bubbles of relativistic plasma which steer the gas during their buoyant rise and simultaneously provide gas heating and mixing.

The toy model makes an optimistic assumption on the efficiency of gas mixing per unit energy. While such mixing efficiency is certainly feasible more detailed simulations (and assumptions on the micro-physics of the ICM) are needed to calculate real efficiency of mixing. We believe, however, that some of these more physically motivated scenarios would have comparable efficiency. For instance, in the recent analysis of metal diffusion in an AGN-driven convection model, Rasera et al. 2008 (see also Chandran & Rasera 2007) predicted the mean AGN luminosity needed to explain the observed abundance profile for M87. They find a mean luminosity of $\sim 10^{43}$ erg s^{-1} which agrees within a factor of a few with our calculation from the toy model.

[6]One should bear in mind that the gas has been already enriched by SNII explosions during an early phase of cluster/galaxy evolution. The metals produced by SNIa during the subsequent evolution are added to this 'minimum' abundance level which amounts to ∼0.1–0.2 of the solar metallicity. This minimum level has to be added to the profiles predicted by our model or subtracted from the observed profiles to make the comparison fair. Because of the large uncertainty in the value of the minimum abundance, we do not do this in Fig. 6 and simply plot the original observed and model profiles.

8 CONCLUSIONS

We consider a simple model of metal spreading through the gaseous atmospheres of cool core clusters due to gas shock heating by a central AGN outburst. In particular, for M87, we show that for the outburst parameters derived from the *Chandra* data (Forman et al. 2007, 2009), the generation of entropy at the shock front by itself does not provide an efficient mechanism for metal transport. However, the energetics of the source are sufficient to spread metals over a large volume (e.g. by entrainment of the metal-rich gas or by steering gas motions in the centre). The assumption that gas mixing and gas heating are closely related to each other leads to a simple qualitative model. The model assumes that full mixing of the gas within a sphere of a given radius occurs on time-scales needed to double the gas thermal energy inside the same sphere. The abundance profile expected in such a simple model demonstrates reasonable similarity to the observed abundance profile in M87 if the time averaged AGN power is of the order of a few $\times\ 10^{43}$ ergs s^{-1}. This value agrees well with the value needed to offset the gas cooling losses in M87.

ACKNOWLEDGMENTS

We are grateful to Hans-Thomas Janka for the provision of one-dimensional Lagrangian hydrodynamics code, initially used for supernovae explosion calculations. This work was supported by the DFG grant CH389/3-2 and the program of the Russian Academy of Sciences 'Origin and evolution of stars and galaxies'.

REFERENCES

Anders E., Grevesse N., 1989, Geochimica et Cosmochimica Acta, 53, 197
Arimoto N., Matsushita K., Ishimaru Y., Ohashi T., Renzini A., 1997, ApJ, 477, 128
Asplund M., Nordlund Å., Trampedach R., Allende Prieto C., Stein R. F., 2000, A&A, 359, 729
Begelman M. C., 2001, in Hibbard J. E., Rupen M., van Gorkom J. H., eds, ASP Conf. Ser. Vol. 240, Gas and Galaxy Evolution: A Conference in Honor of the 20th Anniversary of the VLA. Astron. Soc. Pac., San Francisco, p. 363
Böhringer H., Matsushita K., Churazov E., Finoguenov A., Ikebe Y., 2004, A&A, 416, L21
Buote D. A., 2000, MNRAS, 311, 176
Chandran B. D. G., Rasera Y., 2007, ApJ, 671, 1413

Churazov E., Brüggen M., Kaiser C. R., Böhringer H., Forman W., 2001, ApJ, 554, 261
Churazov E., Sunyaev R., Forman W., Böhringer H., 2002, MNRAS, 332, 729
Churazov E., Forman W., Vikhlinin A., Tremaine S., Gerhard O., Jones C., 2008, MNRAS, 388, 1062
Ciotti L., D'Ercole A., Pellegrini S., Renzini A., 1991, ApJ, 376, 380
De Grandi S., Ettori S., Longhetti M., Molendi S., 2004, A&A, 419, 7
David L. P., Nulsen P. E. J., 2008, ApJ, 689, 837
Finoguenov A., Matsushita K., Böhringer H., Ikebe Y., Arnaud M., 2002, A&A, 381, 21
Forman W. et al., 2005, ApJ, 635, 894
Forman W. et al., 2007, ApJ, 665, 1057
Forman W. et al., 2009, ApJ, to be submitted
Heath D., Krause M., Alexander P., 2007, MNRAS, 374, 787
Hernquist L., 1990, ApJ, 356, 359
Kaiser C. R., Binney J., 2003, MNRAS, 338, 837
Lodders K., 2003, ApJ, 591, 1220
Mannucci F., Maoz D., Sharon K., Botticella M. T., Della Valle M., Gal-Yam A., Panagia N., 2008, MNRAS, 383, 1121
Matsushita K., Belsole E., Finoguenov A., Böhringer H., 2002, A&A, 386, 77
McNamara B. R., Nulsen P. E. J., 2007, ARA&A, 45, 117
Nulsen P. E. J., Jones C., Forman W., David L., McNamara B., Rafferty D., Birzan L., Wise M., 2007, in Böhringer, H., Schuecker P., Pratt G. W., Finoguenov A., eds, Heating vs. Cooling in Galaxies and Clusters of Galaxies. Springer-Verlag, Berlin
Rasera Y., Lynch B., Srivastava K., Chandran B., 2008, ApJ, 689, 825
Rebusco P., Churazov E., Böhringer H., Forman W., 2005, MNRAS, 359, 1041
Rebusco P., Churazov E., Böhringer H., Forman W., 2006, MNRAS, 372, 1840
Renzini A., Ciotti L., D'Ercole A., Pellegrini S., 1993, ApJ, 419, 52
Roediger E., Brüggen M., Rebusco P., Böhringer H., Churazov E., 2007, MNRAS, 375, 15
Romanowsky A. J., Kochanek C. S., 2001, ApJ, 553, 722
Schindler S., Diaferio A., 2008, Space Sci. Rev., 134, 363
Simionescu A., Werner N., Finoguenov A., Böhringer H., Brüggen M., 2008, A&A, 482, 97
Sutherland R. S., Dopita M. A., 1993, ApJS, 88, 253

This paper has been typeset from a TEX/LATEX file prepared by the author.